

Optical observation of the $3s\sigma_g F^3\Pi_u$ Rydberg state of N_2

J. P. Sprengers, E. Reinhold, and W. Ubachs

Laser Centre, Department of Physics and Astronomy, Vrije Universiteit, De Boelelaan 1081, 1081 HV Amsterdam, The Netherlands

K. G. H. Baldwin and B. R. Lewis^{a)}

Research School of Physical Sciences and Engineering, The Australian National University, Canberra ACT 0200, Australia

(Received 22 July 2005; accepted 22 August 2005; published online 13 October 2005)

Using ultrahigh-resolution 1 XUV+1 UV two-photon ionization laser spectroscopy, the $F^3\Pi_u \leftarrow X^1\Sigma_g^+(0,0)$ transition of N_2 has been optically observed for the first time, and the $3s\sigma_g F^3\Pi_u(v=0)$ Rydberg level fully characterized with rotational resolution. The experimental spectroscopic parameters and predissociation level widths suggest strong interactions between the F state and the $3p\pi_u G^3\Pi_u$ Rydberg and $C'^3\Pi_u$ valence states, analogous to those well known in the case of the isoconfigurational $^1\Pi_u$ states. © 2005 American Institute of Physics.
[DOI: 10.1063/1.2062189]

I. INTRODUCTION

Knowledge of N_2 spectroscopy and dissociation dynamics in the extreme ultraviolet (XUV) region is essential for a proper understanding of the radiative and photochemical processes occurring in nitrogen-rich planetary atmospheres. The lowest dipole-allowed transitions from the $X^1\Sigma_g^+$ state of N_2 , which occur above $\sim 100\,000\text{ cm}^{-1}$ in the XUV, result from the excitation of highly mixed Rydberg and valence states of $^1\Pi_u$ and $^1\Sigma_u^+$ symmetry.^{1,2} While these states and their interactions have been well studied, both experimentally and theoretically, their predissociation mechanisms are not well understood. For example, although it has been confirmed very recently that the lowest $^1\Pi_u$ states of N_2 predissociate by spin-orbit coupling to the $^3\Pi_u$ manifold,³ experimental information on the spectroscopy and dissociation dynamics of the relevant $^3\Pi_u$ states is very limited. In particular, lack of information on the $^3\Pi_u$ Rydberg states has restricted the N_2 predissociation model of Ref. 3 to a consideration of only the lowest $^1\Pi_u$ levels.

The lowest Rydberg states of N_2 which are members of a series converging on the $X^2\Sigma_g^+$ core of N_2^+ are the well-known *gerade* states $3s\sigma_g a''^1\Sigma_g^+$ and $3s\sigma_g E^3\Sigma_g^+$, with $v=0$ levels near $99\,000$ and $96\,000\text{ cm}^{-1}$, respectively.⁴ The lowest *ungerade* Rydberg states arise from the $3p$ complex⁵ in the $103\,000$ – $105\,000\text{ cm}^{-1}$ energy region, comprising $3p\sigma_u c'^1\Sigma_u^+$, $3p\sigma_u D^3\Sigma_u^+$, $3p\pi_u c^1\Pi_u$, and $3p\pi_u G^3\Pi_u$. While only the first three of these states are known from optical spectroscopy,⁴ the nomenclature G for the $^3\Pi_u$ state has been employed for some time,^{6–10} somewhat confusingly, given the use of the same nomenclature for the $^3\Delta_g$ valence state of N_2 near $88\,000\text{ cm}^{-1}$.⁴ The lowest Rydberg states of N_2 which are members of series converging on the $A^2\Pi_u$ core of N_2^+ are the $3s\sigma_g o^1\Pi_u$ and $3s\sigma_g F^3\Pi_u$ states, in the $105\,000$ – $106\,000\text{ cm}^{-1}$ energy region. The c and o states are the Rydberg members of the $^1\Pi_u$ manifold accessed in the

first allowed transitions of N_2 , while the F and G states are the Rydberg members of the $^3\Pi_u$ manifold responsible for the $^1\Pi_u$ predissociation.

The $^3\Pi_u \leftarrow X^1\Sigma_g^+$ transitions of N_2 are optically forbidden and the only previously published assignments of levels of the F and G states have been in low-resolution electron-energy-loss,^{6–8} (EEL) and photofragment,⁹ (PF) spectra. These assignments, which were not based on rotational analyses since the applicable experimental bandwidths were $\geq 200\text{ cm}^{-1}$ full width at half maximum (FWHM), must, therefore, remain in doubt. In particular, the question of the vibrational numbering of the $F(v)$ levels has been controversial, with Leoni and Dressler¹⁰ invoking a diffuse $F(v=0)$ level near $102\,900\text{ cm}^{-1}$ in order to explain the strong predissociation of the $b^1\Pi_u(v=3)$ valence level, while Robbe¹¹ argued against this assignment, suggesting, on theoretical grounds, that the $F(v=0)$ level lay at a significantly higher energy. This matter has been settled convincingly only by the PF study of van der Kamp *et al.*,⁹ who found the $F(v=0)$ level at $104\,500(160)\text{ cm}^{-1}$.¹²

Here, we present the results of an ultrahigh-resolution laser-spectroscopic study of the $F \leftarrow X(0,0)$ transition of $^{14}N_2$. This dipole-forbidden transition becomes observable, apparently through the indirect spin-orbit borrowing of intensity from the dipole-allowed $b \leftarrow X(5,0)$ transition, facilitated by the near degeneracy of the $F(v=0)$ and $b(v=5)$ levels in the normal isotopomer. This study represents the first reported observation of the F state in an optical transition and is the first to provide spin- and rotationally resolved spectroscopic data. In addition, the excellent experimental resolution enables the $F(v=0)$ predissociation level widths to be determined for the first time, information expected to be crucial to the extension of N_2 predissociation models to higher energies than presently applicable.

II. EXPERIMENTAL METHOD

The experimental setup was similar to the system used in our previous ultrahigh-resolution laser-spectroscopic studies

^{a)}Electronic mail: brenton.lewis@anu.edu.au

of N_2 ,^{13,14} except that the system was modified and significantly improved in order to observe the extremely weak signal levels expected for a dipole-forbidden transition, such as $F \leftarrow X(0,0)$. Briefly, a narrowband tunable cw-ring dye laser, pumped by a 532 nm Millennia-V laser, injection seeded a pulsed dye amplifier (PDA). The Nd:YAG pump laser for the PDA was changed from a Spectra-Physics GCR-5 to a Spectra-Physics GCR-330, which gives higher energies (750 mJ per pulse and 1 J per pulse, respectively) and has a better beam profile. The PDA configuration was slightly changed to improve the overlap of the pump beam with the seed laser in the dye cells. A carefully optimized mixture of rhodamine 6G and rhodamine B was used as dye mixture in the PDA, since the dyes individually did not cover the required wavelength range (572.0–573.5 nm). A KD*P crystal frequency doubled the output of the PDA into the UV and, subsequent frequency tripling in a pulsed N_2 jet generated XUV radiation. In our previous experiments, a xenon jet was used but, at these particular wavelengths (95.40–95.55 nm), more XUV was produced with N_2 as the tripling medium. These changes and optimizations resulted in typical UV powers of 50 mJ per pulse. The collinearly propagating XUV and remaining UV beams were crossed with a pulsed N_2 jet in a separate chamber where the spectroscopic measurements were performed. The $F \leftarrow X(0,0)$ band was recorded using 1 XUV+1 UV two-photon ionization spectroscopy, where the XUV photon accessed the $F \leftarrow X$ transition and, subsequently, the UV photon ionized the excited molecules. The resultant N_2^+ ions were detected in a time-of-flight electron-multiplier detection system. The distance between the nozzle and the skimmer was decreased to a few millimeters to increase the ion signal. This resulted in the N_2 gas pressure increasing in the interaction chamber to 4×10^{-5} mbar, with typical pressures of 3 bars behind the nozzle. Only with this nozzle-skimmer configuration and gas pressure were N_2^+ ions corresponding to $F(v=0)$ excitation detected. An étalon and an I_2 -saturated absorption setup provided absolute frequency calibration, which was performed in the visible using the output of the cw-ring dye laser.

In Fig. 1, the instrumental width of the experimental system is demonstrated using a scan over the $R(1)$ line of the $b' \leftarrow X(2,0)$ transition in $^{14}N_2$, performed under the same experimental conditions as for the $F \leftarrow X(0,0)$ measurements. This line was measured also with the nozzle located 10 cm from the skimmer and compared with scans over low-rotational lines from the $b \leftarrow X(1,0)$ band. The $b(v=1)$ level in $^{14}N_2$ is long lived [$\tau=2610(100)$ ps] (Ref. 15) and, therefore, the experimental widths of lines reaching this level are mainly instrument limited.¹³ The $R(1)$ line of $b' \leftarrow X(2,0)$ was, with the nozzle at 10 cm, only marginally broader than the $b \leftarrow X(1,0)$ lines. Therefore, the scan over the $b' \leftarrow X(2,0)$ line in Fig. 1 essentially defines the instrumental width applicable to the $F \leftarrow X(0,0)$ measurements. Fitting of a Voigt profile to the scan (effective resolution 0.057 cm^{-1} FWHM) yielded a Doppler component of $0.041(1) \text{ cm}^{-1}$ FWHM, together with a Lorentz component of $0.029(2) \text{ cm}^{-1}$ FWHM. These values were used in the analysis of all experimental $F \leftarrow X(0,0)$ profiles.

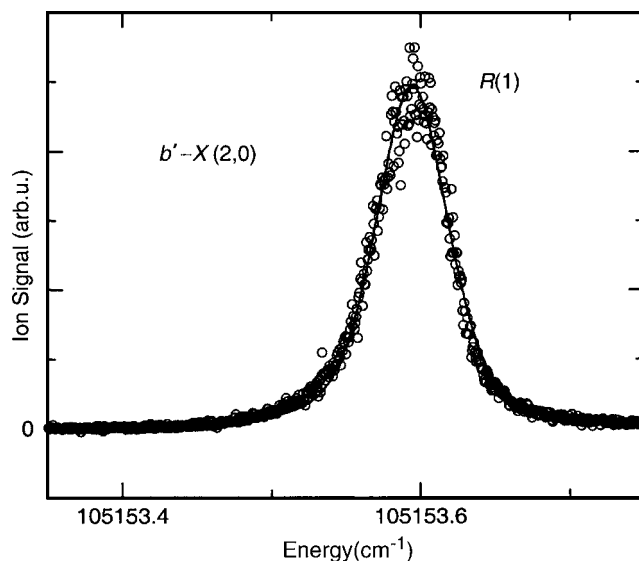


FIG. 1. 1 XUV+1 UV ionization spectrum of the $R(1)$ line of the $b' \leftarrow X(2,0)$ band in $^{14}N_2$ (open circles), recorded under the same experimental conditions as used for the $F \leftarrow X(0,0)$ measurements, fitted with a Voigt profile (solid line). The very small asymmetry of the line is possibly due to a slight misalignment of the nozzle and skimmer.

III. RESULTS AND DISCUSSION

In a number of short experimental scans over the region $104\ 705\text{--}104\ 765 \text{ cm}^{-1}$, we observed structure which, as will become clear, was due to the $F \leftarrow X(0,0)$ transition. These results are summarized in the composite spectrum of Fig. 2, in which some channel averaging has been performed for clarity, while not significantly compromising the widths of the narrowest features. The $F \leftarrow X(0,0)$ lines are notably diffuse, characterized by near-Lorentzian line shapes, indicating

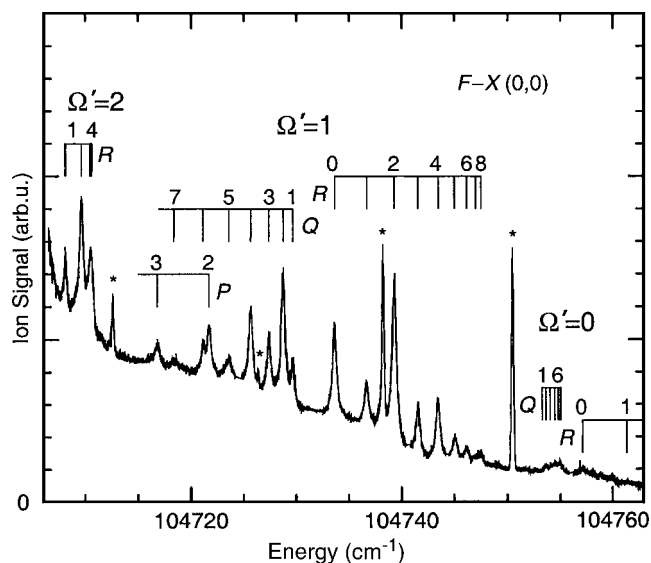


FIG. 2. Composite 1 XUV+1 UV ionization spectrum of the $F \leftarrow X(0,0)$ band of $^{14}N_2$, including partial line assignments for the three spin subbands. The P and Q branches of the low-energy subband are not detectable, as they are obscured by the rapidly rising signal from the dipole-allowed transition $b \leftarrow X(5,0)$ (extreme left of figure), while the higher R -branch lines in the high-energy subband are too weak to observe (extreme right of figure). Narrower lines marked with an asterisk are high-rotational lines from higher-lying dipole-allowed transitions (see text).

a strong degree of predissociation of the $F(v=0)$ level. Four narrower lines, marked with asterisks in Fig. 2, contaminate the spectrum. These lines have distinctly different profiles from the $F\leftarrow X(0,0)$ lines, and are characterized by an essentially Gaussian line shape with a FWHM of $\sim 0.25\text{ cm}^{-1}$, corresponding to the room-temperature Doppler profile of the N_2 background gas. They are high-rotational lines from higher-lying allowed transitions, specifically, $P(21)$, $R(23)$, and $P(20)$ from the $b'\leftarrow X(2,0)$ band, at $104\,712.61\text{ cm}^{-1}$, $104\,738.27\text{ cm}^{-1}$, and $104\,750.48\text{ cm}^{-1}$, respectively, and $P(29)$ from the $b\leftarrow X(6,0)$ band at $104\,726.37\text{ cm}^{-1}$.

The clearest features in Fig. 2 are P , Q , and R branches in the central region, near $104\,730\text{ cm}^{-1}$. Combination differences confirm that these arise from the ground state of $^{14}N_2$, and they can be associated with the central $F(v=0, \Omega=1)\leftarrow X(v=0)$ subband. In the low-energy region of Fig. 2, near $104\,710\text{ cm}^{-1}$, a returning R branch can be identified, corresponding to the $F(v=0, \Omega=2)\leftarrow X(v=0)$ subband, since we could not find any corresponding $R(0)$ transition. Finally, in the high-energy region of Fig. 2, near $104\,755\text{ cm}^{-1}$, an overlapped Q head, together with $R(0)$, and, possibly, $R(1)$ lines, appear very weakly, corresponding to the $F(v=0, \Omega=0)\leftarrow X(v=0)$ subband. These observations confirm that the $^3\Pi_u$ upper state of the observed transition is inverted, as indeed expected for the $3s\sigma_g F^3\Pi_u$ Rydberg state, the first member of a series converging on the first excited state of N_2^+ , a $^2\Pi_u$, which is known to be inverted.¹⁶

The individual scan segments in Fig. 2 were not all performed with the same experimental sensitivity. Nevertheless, it was clear that the subband intensities decreased significantly as their energy increased, consistent with the view that the $F\leftarrow X(0,0)$ transition borrows its intensity from the lower-lying dipole-allowed $b\leftarrow X(5,0)$ transition. For example, the $b(v=5)$ level at $104\,700\text{ cm}^{-1}$ is nearly degenerate with the $F(v=0, \Omega=2)$ sublevel, but some 50 cm^{-1} lower in energy than $F(v=0, \Omega=0)$, leading to much greater intensity borrowing in the former case. The most likely coupling mechanism leading to the intensity borrowing is indirect spin-orbit coupling between the $b^1\Pi_u(v=5, \Omega=1)$ and $F^3\Pi_u(v=0, \Omega=1)$ levels, assisted by rotation-dependent S uncoupling between the F -state triplet sublevels.

In order to obtain precise experimental line positions and predissociation widths, we performed Voigt profile analyses on the individual $F\leftarrow X(0,0)$ lines, using a least-squares fitting procedure and correcting for the effects of instrumental resolution, including Doppler broadening. A typical fit is shown in Fig. 3, for the case of the $R(0)$ line of the central subband, yielding a residual Lorentzian linewidth of 0.45 cm^{-1} FWHM, attributable to predissociation. In the case of significantly overlapped pairs of lines, e.g., the $R(3)$ and $R(4)$ lines of the lower subband, the individual linewidths were tied to a single value, determined by the fit, together with the individual line positions, albeit with greater uncertainties. In the case of the Q branch of the upper subband, which contains six lines, the individual line spacings were fixed according to an initial estimate of the appropriate F -state rotational constant, and a single linewidth and overall position were determined by the fit, nominally associated

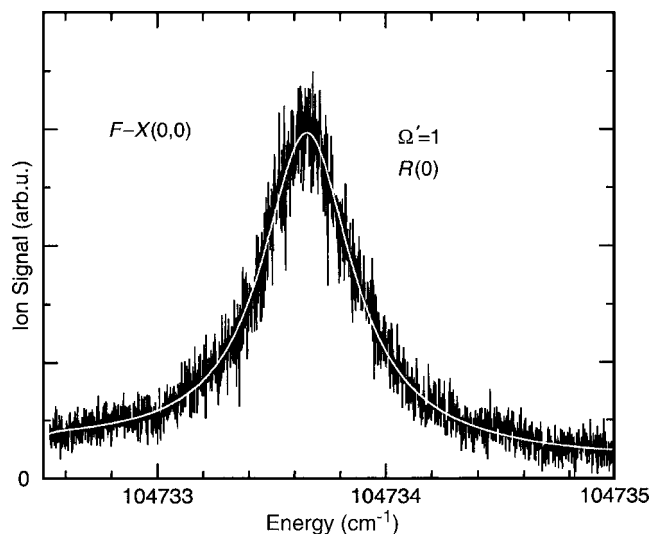


FIG. 3. Typical ionization spectrum of the $R(0)$ line of the central $F\leftarrow X(0,0)$ subband (solid line), fitted with a Voigt profile (open line). Assumption of an instrumental profile as in Fig. 1 yields a predissociation linewidth of 0.45 cm^{-1} FWHM.

with the $Q(2)$ line, the peak of which was distinguishable in the experimental spectrum. The resultant experimental line positions and predissociation linewidths are summarized in Tables I and II, respectively, the greater uncertainties associated with the analysis of blended or weak features. Finally, the transition wave numbers in Table I were combined with the appropriate $^{14}N_2$ ground-state terms,¹⁷ to form rotational term values for the $F(v=0)$ state, which were then fitted using the $^3\Pi$ Hamiltonian of Brown and Merer,¹⁸ yielding the spectroscopic parameters given in Table III.

The experimental $F(v=0)$ -state energy in Table III, $\nu_0 = 104\,727\text{ cm}^{-1}$, differs from previous PF (Ref. 9) and EEL (Refs. 6–8 and 19) values by ~ 230 and $\sim 10\text{--}40\text{ cm}^{-1}$, respectively, differences within, or similar to, the combined

TABLE I. Wave numbers for rotational lines observed in the $F^3\Pi_u\leftarrow X^1\Sigma_g^+(0,0)$ band system of $^{14}N_2$, in cm^{-1} . Uncertainties include calibration and statistical contributions.

Ω'	J''	$P(J'')$	$Q(J'')$	$R(J'')$
0	0			104 757.133(17)
	1			104 761.406(35)
	2	104 745.180(35)	104 753.636(17)	
1	0			104 733.656(11)
	1		104 729.664(12)	104 736.703(11)
	2	104 721.711(11)	104 728.742(11)	104 739.336(11)
	3	104 716.820(13)	104 727.398(11)	104 741.570(11)
	4		104 725.672(11)	104 743.469(11)
	5		104 723.578(19)	104 744.992(28)
	6		104 721.141(12)	104 746.156(12)
	7		104 718.359(25)	104 747.016(32)
2	8			104 747.500(32)
	1			104 708.117(12)
	2			104 709.641(11)
	3			104 710.438(19)
	4			104 710.625(18)
	5			104 710.117(30)

TABLE II. Experimental predissociation level widths for the $F^3\Pi_u(v=0)$ state of $^{14}\text{N}_2$, in cm^{-1} FWHM.

J	$\Omega=0$		$\Omega=1$		$\Omega=2$
	Γ_e	Γ_f	Γ_e	Γ_f	Γ_e
1	0.57(8)		0.45(3)	0.41(4)	
2			0.45(3)	0.45(3)	0.35(3)
3			0.46(3)	0.45(4)	0.40(3)
4		0.48(6)	0.48(4)	0.45(3)	
5			0.51(4)	0.45(5)	0.39(4)
6			0.49(10)	0.34(4)	
7			0.46(5)	0.46(10)	

experimental uncertainties in each case, but the present measurement is much more precise. The rotational constant, $B = 1.803 \text{ cm}^{-1}$, is consistent with our Rydberg-state assignment, but is a little greater than expected for a Rydberg state built on the $A^2\Pi_u$ ionic core [$B(A, v=0) = 1.735 \text{ cm}^{-1}$],⁴ suggesting significant mixing with a state carrying a higher rotational constant, such as the $3p\pi_u G^3\Pi_u$ Rydberg state, the lowest member of a series converging on the $X^2\Sigma_g^+$ ionic core [$B(X, v=0) = 1.922 \text{ cm}^{-1}$].⁴ The spin-orbit coupling constant, $A = -21.8 \text{ cm}^{-1}$, while consistent with the expectation of an inverted F state, has a magnitude somewhat less than that expected for a Rydberg $^3\Pi_u$ state built on the $A^2\Pi_u$ ionic core, i.e., $A \approx \frac{1}{2}A[\text{N}_2^+(A^2\Pi_u)] \approx -37 \text{ cm}^{-1}$,^{3,5} suggesting mixing with a state having a more positive A value. This difference is also consistent with mixing between the F and G states, since a Rydberg $^3\Pi_u$ state built on the $X^2\Sigma_g^+$ ionic core would be expected to have $A = a_{3p\pi_u} \approx \zeta_{3p_N} \approx +2 \text{ cm}^{-1}$.^{3,5,20}

The mixing postulated above between the F and G states can be confirmed semiquantitatively. If we consider a simple two-level interaction between “pure” Rydberg $F(v=0)$ and $G(v=0)$ states having $B = 1.735 \text{ cm}^{-1}$, $A = -37 \text{ cm}^{-1}$, and $B = 1.922 \text{ cm}^{-1}$, $A = +2 \text{ cm}^{-1}$, respectively, with leading wavefunction coefficients of 0.82,²¹ then the effective values for the mixed F level will become $B = (0.82^2)(1.735) + (1 - 0.82^2)(1.922) = 1.796 \text{ cm}^{-1}$, and, by similar reasoning, $A = -24.2 \text{ cm}^{-1}$. These values are in good agreement with our experimental values of 1.803 and -21.8 cm^{-1} , respectively. Similarly, the effective values for the correspondingly mixed G level will be $B = 1.861 \text{ cm}^{-1}$ and $A = -10.8 \text{ cm}^{-1}$, the G

state becoming *inverted* due to the interaction. We have recently become aware of an unpublished ultrahigh-resolution study of the $G^3\Pi_u \leftarrow E^3\Sigma_g^+(0,0)$ transition, using near-infrared diode-laser spectroscopy, which yielded the results $B = 1.864 \text{ cm}^{-1}$ and $A = -8.17 \text{ cm}^{-1}$, for the $G(v=0)$ level.^{22,23} So, our two-level model of strong mixing between $F(v=0)$ and $G(v=0)$ is in good agreement also for the G state.

Using similar arguments, it is possible also to explain the observed value of λ in Table III. The effective spin-spin constant $\lambda^{\text{eff}} = \lambda^{\text{SS}} + \lambda^{\text{SO}}$, where λ^{SS} is the true spin-spin constant and λ^{SO} is the contribution from second-order isoconfigurational spin-orbit interaction.⁵ Semiempirical estimates⁵ in the case of the pure $\pi_u \sigma_g F^3\Pi_u(v=0)$ state yield: $\lambda^{\text{SS}} = -3\eta/2 = -0.21 \text{ cm}^{-1}$, where $\eta = 0.14 \text{ cm}^{-1}$ is the atomic spin-spin parameter for N ,⁵ $\lambda^{\text{SO}} = A^2/2\Delta E = 0.72 \text{ cm}^{-1}$, where $A = -37 \text{ cm}^{-1}$ is the spin-orbit constant for the pure F state and $\Delta E = 950 \text{ cm}^{-1}$ is the energy separation between the isoconfigurational $F^3\Pi_u(v=0)$ and $o^1\Pi_u(v=0)$ levels; and thus $\lambda^{\text{eff}} = 0.51 \text{ cm}^{-1}$. In the case of the pure $\sigma_g \pi_u G^3\Pi_u(v=0)$ state, $\lambda^{\text{eff}} = \lambda^{\text{SS}} = -0.21 \text{ cm}^{-1}$,⁵ since λ^{SO} is negligible, owing to the low A value for the G state, which is a member of a Rydberg series converging on a closed-shell ionic core. If we now introduce the mixing postulated above between the $F(v=0)$ and $G(v=0)$ states, in the case of the mixed F state, we find $\lambda^{\text{eff}} = (0.82^2)(0.51) + (1 - 0.82^2)(-0.21) = +0.27 \text{ cm}^{-1}$, in good agreement with the experimental value of 0.30 cm^{-1} in Table III, and confirming the dominant role of λ^{SO} , which certainly determines the sign of the observed effective spin-spin constant. Similarly, in the case of the mixed G state, $\lambda^{\text{eff}} = +0.03 \text{ cm}^{-1}$, in good agreement with the experimental value of Ref. 22 (-0.011 cm^{-1}). Thus, in this latter case, the true spin-spin constant of the pure G state is essentially counterbalanced by the isoconfigurational spin-orbit contribution borrowed from the F state, giving a near-zero effective value. Overall, it is clear that a simple $\sim 2:1$ mixing between the $F(v=0)$ and $G(v=0)$ levels is all that is needed to semiquantitatively explain the observed B , A , and λ values for each level.

The experimental predissociation level widths in Table II show little rotational dependence, no e/f -parity dependence, and only a slight tendency to decrease as Ω increases from 0 to 2. The most likely predissociation mechanism is electrostatic interaction with the $C' ^3\Pi_u$ valence state, rather than a spin-orbit process. The C' potential-energy curve crosses the outer limb of the F -state curve well above the $v=0$ level,³ so

TABLE III. Experimental spectroscopic parameters for the $F^3\Pi_u(v=0)$ state of $^{14}\text{N}_2$, in cm^{-1} .

Param.	This work	Previous work
ν_0	104 727.41(10) ^a	$\nu_0 = 104 500(160)$ ^b
B	1.8028(1)	$\nu_0 = 104 690(40)$ ^c
A	-21.82(1)	$\nu_0 = 104 690(40)$ ^d
λ	0.302(3)	$\nu_0 = 104 740(40)$ ^e
o	0.072(5)	
p	0.0046(14)	
q	-0.0021(8)	

^aRotationless F_2 energy = $\nu_0 - 4\lambda/3 + 2B = 104 730.61(10) \text{ cm}^{-1}$.^bReference 9.^cReference 6.^dReference 7.^eReference 8.

a strong, possibly multistate, interaction will be required to explain the large average experimental predissociation level width of $\sim 0.45 \text{ cm}^{-1}$ FWHM.

IV. SUMMARY AND CONCLUSIONS

We have optically observed the $F \leftarrow X(0,0)$ transition for the first time and characterized the $3s\sigma_g F^3\Pi_u(\nu=0)$ Rydberg level with rotational resolution. The experimental spectroscopic parameters and predissociation level widths suggest strong interactions between the F state and the $3p\pi_u G^3\Pi_u$ Rydberg and $C'^3\Pi_u$ valence states, analogous to those well known in the case of the isoconfigurational $^1\Pi_u$ states.¹⁻³ This new experimental information will prove valuable in the extension of existing N_2 coupled-channel predissociation models³ to higher energies.

ACKNOWLEDGMENTS

The Molecular Atmospheric Physics (MAP) Program of the Netherlands Foundation for Fundamental Research on Matter (FOM), and the Discovery Program of the Australian Research Council are gratefully acknowledged for their support. One of the authors (JPS) thanks the ANU for the hospitality enjoyed during a visit to Canberra. Another author (BRL) thanks Professor H. Kanamori, for the supply of Ref. 22, and Professors G. Stark and K. Yoshino, for the provision of a spectroscopic plate on which we found fragments of the $F \leftarrow X(0,0)$ band, inspiring the present study.

¹D. Stahel, M. Leoni, and K. Dressler, J. Chem. Phys. **79**, 2541 (1983).

²D. Spelsberg and W. Meyer, J. Chem. Phys. **115**, 6438 (2001).

³B. R. Lewis, S. T. Gibson, W. Zhang, H. Lefebvre-Brion, and J.-M. Robbe, J. Chem. Phys. **122**, 144302 (2005).

⁴K. P. Huber and G. Herzberg, *Molecular Spectra and Molecular Structure IV. Constants of Diatomic Molecules* (Van Nostrand, New York, 1979), pp. 414–426.

⁵H. Lefebvre-Brion and R. W. Field, *The Spectra and Dynamics of Diatomic Molecules* (Elsevier, Amsterdam, 2004), pp. 183–190, 196–202, 315–322, 399–400.

⁶J. Mazeau, R. I. Hall, G. Joyez, M. Landau, and J. Reinhardt, J. Phys. B **6**, 873 (1973).

⁷G. Joyez, R. I. Hall, J. Reinhardt, and J. Mazeau, J. Electron Spectrosc. Relat. Phenom. **2**, 183 (1973).

⁸P. Hammond, G. C. King, J. Jureta, and F. H. Read, J. Phys. B **20**, 4255 (1987).

⁹A. B. van der Kamp, P. C. Cosby, and W. J. van der Zande, Chem. Phys. **184**, 319 (1994).

¹⁰M. Leoni and K. Dressler, Z. Angew. Math. Phys. **22**, 794 (1971).

¹¹J. M. Robbe, Ph.D. thesis, University of Lille, 1978.

¹²Throughout this work, numbers in parentheses represent 1σ uncertainties, in units of the least significant figure.

¹³J. P. Sprengers, W. Ubachs, and K. G. H. Baldwin, J. Chem. Phys. **122**, 144301 (2005).

¹⁴J. P. Sprengers, W. Ubachs, K. G. H. Baldwin, B. R. Lewis, and W.-Ü L. Tchang-Brillet, J. Chem. Phys. **119**, 3160 (2003).

¹⁵J. P. Sprengers, W. Ubachs, A. Johansson, A. L'Huillier, C.-G. Wahlström, R. Lang, B. R. Lewis, and S. T. Gibson, J. Chem. Phys. **120**, 8973 (2004).

¹⁶A. E. Douglas, Astrophys. J. **117**, 380 (1953).

¹⁷M. L. Orlov, J. F. Ogilvie, and J. W. Nibler, J. Mol. Spectrosc. **185**, 128 (1997).

¹⁸J. M. Brown and A. J. Merer, J. Mol. Spectrosc. **74**, 488 (1979).

¹⁹The previous EEL studies had misassigned $F(\nu=0)$ as $F(\nu=1)$.

²⁰ a and ζ are single-electron molecular and atomic spin-orbit parameters, respectively.

²¹A coefficient of 0.82 results in the best overall fit of this simple model to experiment.

²²T. Hashimoto, MS thesis, Tokyo Institute of Technology, 1996; T. Hashimoto and H. Kanamori, J. Mol. Spectrosc. (submitted).

²³The Ref. 22 B value for the $G(\nu=0)$ state has been adjusted to be consistent with the same Brown and Merer Hamiltonian (Ref. 18) that we have used here for analysis of the $F(\nu=0)$ state.